Geosynthetics Conference

Asphalt Strain Response of Geosynthetic-Reinforced Asphalt Overlays under Static Plate Loads

V. Vinay Kumar, Ph.D.,[1] Gholam H. Roodi, Ph.D.,[2] and Jorge G. Zornberg, Ph.D., P.E.[3]

[1]Department of Civil, Architectural and Environmental Engineering, University of Texas at Austin, Austin, Texas-78712; e-mail: vinay.vasanth@utexas.edu
[2]Department of Civil, Architectural and Environmental Engineering, University of Texas at Austin, Austin, Texas-78712; e-mail: hroodi@utexas.edu
[3]Department of Civil, Architectural and Environmental Engineering, University of Texas at Austin, Austin, Texas-78712; e-mail: zornberg@mail.utexas.edu

ABSTRACT

Geosynthetic interlayers have proven successful in retarding the rate of reflective crack development in asphalt overlays. In addition, geosynthetic interlayers are also expected to enhance the structural capacity of pavements (e.g., by retarding the development of permanent deflections and tensile strains within the asphalt layers). However, the relevant mechanisms leading to an enhanced performance of geosynthetic-reinforced asphalt layers are not clearly understood and the structural benefits from geosynthetics are yet to be quantified. In this study, the asphalt strain response in full-scale field test sections comprising both unreinforced (control) and geosynthetic-reinforced asphalt overlay test sections was evaluated using static plate load tests. The road sections included an oxidized old asphalt layer and rehabilitation involved placing tack coat, installing geosynthetic interlayer (only in the geosynthetic-reinforced section), and finally constructing a 3-inch-thick asphalt overlay. The asphalt strains were recorded by the asphalt strain gauges installed at a depth of 3 inches within the old asphalt layer, under a static plate load application. Comparison of settlement and asphalt strain response of geosynthetic-reinforced overlay section with that of control section indicates that the geosynthetic reinforcements significantly reduced tensile strains in the asphalt layers. Specifically, under the same plate loads, the tensile strains in the geosynthetic-reinforced section was at least 90% less than the tensile strains in the unreinforced (control) section.

INTRODUCTION

A wide range of pavement interlayers have been used to enhance the performance of the asphalt overlays. The main functions that have been expected from using pavement interlayers include waterproofing, stress relieving and reinforcement (Lytton 1989). Engineering fabrics (such as geotextiles) and geocomposites have been typically used to provide waterproofing and stress relieving while grid-structure interlayers (such as geogrids and glass grid materials) have been mostly used to provide reinforcement function. However, specific conditions in which the benefits from each type of interlayers are realized are still unclear and need further investigation.

A wide range of experimental procedures have been used to evaluate performance of pavement interlayers. Examples include bond strength tests (e.g., Canestrari et al. 2005; Kumar et al. 2017; Leutner 1979; Roodi et al. 2017; West et al. 2005), flexural beam tests (e.g., Khodaii et al. 2009; Kumar and Saride 2017; Montestruque et al. 2004; Pasquini et al. 2014), and physical

pavement model tests (e.g., Correia and Zornberg 2016; Saride and Kumar 2019). Pavement models have been loaded using plate load setup, wheel loads, or accelerated pavement loading facilities. However, comparatively limited field trials have been conducted to explore the reinforced asphalt performance (e.g., Zou et al. 2007).

This study presents the results of static plate load tests conducted on a highway section in Texas. The roadway was tested before and after construction of an asphalt overlay. The tests were conducted at two locations including a location where a geocomposite interlayer was placed between the old and new asphalt and a location where no interlayer was placed. The settlement under the plate load test as well as tensile strain in the old asphalt were evaluated between the two sections.

PAVEMENT SECTIONS AND INSTRUMENTATION

As part of a rehabilitation plan along a long section of State Highway 21 in Texas, a 3-inch-thick asphalt overlay was constructed over the existing pavement. As part of this research study, a short section of the construction was used to investigate effectiveness of using pavement interlayers. Specifically, two different pavement interlayer systems were tested at two sections under static plate load test. In Section 1, referred to as the control section (CS), no pavement interlayer was used while in Section 2, referred to as the GG section, a geocomposite interlayer was used.

The road profile at the two tested locations were investigated by drilling from the pavement surface through the subgrade. Figures 1a and b show the road profile in Sections 1 and 2, respectively. The thickness of the old asphalt was 6 and 5 inches in Sections 1 and 2, respectively. The thickness of the base and subbase courses were 6 and 10 inches in Section 1, respectively, and 7 and 9 inches in Section 2, respectively. The old asphalt, base course and subbase course had similar characteristics in the two sections. The new asphalt included a 2-inch-thick Type D mix overlain by a 1-inch-thick thin overlay mix (TOM), classified according to Texas Department of Transportation (TxDOT) Standard Specifications for Construction and Maintenance of Highways, Streets, and Bridges (TxDOT 2014).

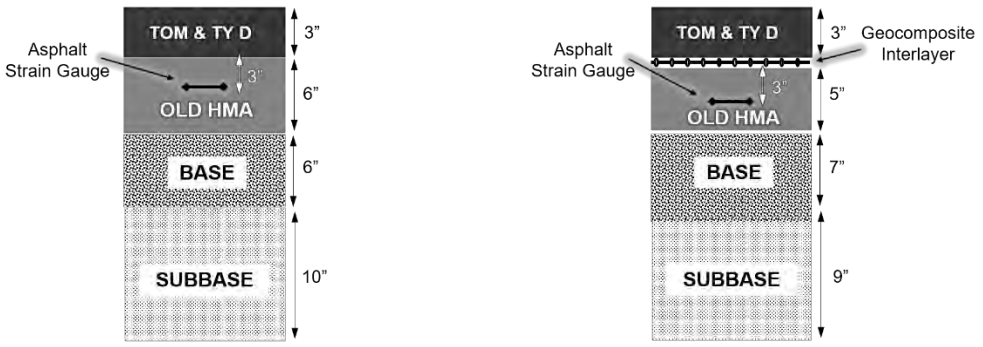

Figure 1. Roadway profile at test sections: a) Section 1 (control section); b) Section 2 (reinforced section).

The interlayer material that was used in Section 2 was a geocomposite consisting of a glass-fiber grid backed by a thin layer of fabric. The geocomposite (GG) had a coating with 60% bitumen content and an ultimate tensile strength of 100 kN/m at 3% strain in both machine and cross-machine directions.

Before construction of the new overlay, H-shaped asphalt strain gauge (Figure 2) was installed at a depth of 3 inch in the old asphalt. To install the asphalt strain gauges, cores were drilled to reach the desired depth in the old asphalt; then, a thin bed of sand-bitumen mix was placed in the bottom of the core, and the core was filled with Type D asphalt mix following placement of the asphalt strain gauges. The asphalt strain gauges were made of high temperature resistance material and included a full-bridge configuration of strain gauges in the web of the H-shaped sensor. The sensors were coated with bitumen to improve contact with surrounding asphalt mix.

Figure 2. Typical asphalt strain gauge installed in the old asphalt.

EXPERIMENTAL PROGRAM

The test sections were loaded using a static plate device before and after construction of the overlay. The plate load tester device, provided by Humboldt, conformed to specifications required by DIN 18134:2012-04 standard (DIN18134, 2012). The testing plate had a diameter of 300 mm and a thickness of 25 mm.

The loading system consisted of a hydraulic pump connected to a hydraulic jack via a high-pressure hose. One end of the hydraulic jack was placed on the loading plate and the other end was secured against a heavy truck for reaction. Both ends had a hinged connection and a load cell was placed between the hydraulic jack and the settlement plate to measure the applied load. The system was capable of applying, maintaining, and releasing the load in controlled stages. The load capacity of the system was 50 kN, equivalent of an applied stress of 0.7 MPa.

The settlement measurement system included a support frame resting on a three-point bearing support. A rotatable rigid contact arm was mounted onto the support frame and could be extended for 1.5 m to reach the loading plate. The end of the contact arm could be adjusted at the center of the plate through a measuring tunnel designed on the plate. A displacement transducer was mounted onto the support frame and attached to the free end of the contact arm to record the settlement. The above system could measure the settlement with a resolution of 0.01 mm. Figure 3 shows a picture of static plate load setup used in this study.

The static plate load tests were conducted in two phases exactly on the same locations, including before (Phase 1) and after (Phase 2) construction of the overlay. In both phases, a seating load of 0.01 MPa were applied to the pavement surface in the beginning of the test. In the first phase (before overlay construction), consistent with DIN 18134:2012-04, the test sections were loaded in six approximately equal increments of 0.08 MPa to reach the maximum stress of 0.5 MPa. Each loading stage was completed within one minute and after a waiting period of 120 seconds, the plate settlement was recorded. Asphalt strain gauges had not yet been installed in this phase; thus, the plate settlement was the only measurement made.

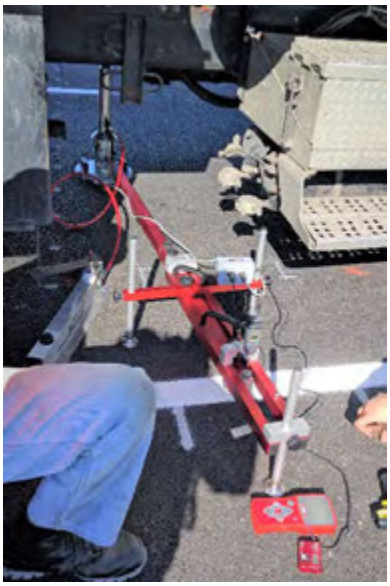

Figure 3. Static Plate Load setup used in the study.

The loading in the second phase of the test (after overlay construction) was identical to the first phase except for the maximum stress. The maximum stress in the second phase was limited to 0.24 MPa, which was applied in three approximately equal increments of 0.08 MPa. In addition, asphalt strain gauges had been installed in this phase; hence, the tensile strain in the old asphalt layer was measured for each loading stage in addition to the plate settlement.

RESULTS AND DISCUSSION

The pavement response under a static plate load test (PLT) is generally presented in a typical load-settlement plot. In addition, the time corresponding to each load and unload stage was carefully recorded in this study. The settlement response corresponding to each load and unload stages were then correlated with the corresponding response recorded from the asphalt strain gauges, as a function of time. Figures 4 and 5 present the 'Time-settlement' and 'Time-strain' recorded under a typical static PLT adopted, for the control and geosynthetic reinforced pavement test sections, respectively. It can be observed that the time corresponding to a settlement is almost the same as that of strain, suggesting a good correlation between the settlement and strains recorded. In addition, both, settlement and tensile strain increased with an increase in the applied load and vice-versa. However, the settlement in the control section (Fig. 4a) is consistently lower than that of geosynthetic reinforced section (Fig. 5a), while the tensile strains in the control section (Fig. 4b) is consistently higher than that of the geosynthetic-reinforced section (Fig. 5b), under the same loading and unloading stages. This condition could be attributed to the influence of ambient and surface temperature during the test and the pre-existing pavement conditions in the control and geosynthetic-reinforced test sections, which will be discussed in next sections of this paper. The average asphalt surface temperature during the static PLT conducted on the control and geosynthetic-reinforced sections were 15 °C (59 °F) and 22 °C (72 °F), respectively.

Besides, another important observation from 'Time-strain' plots (Figs. 4b & 5b) suggest that the strains recorded under a typical load/unload stage did not completely stabilize, before proceeding to the next load stage.

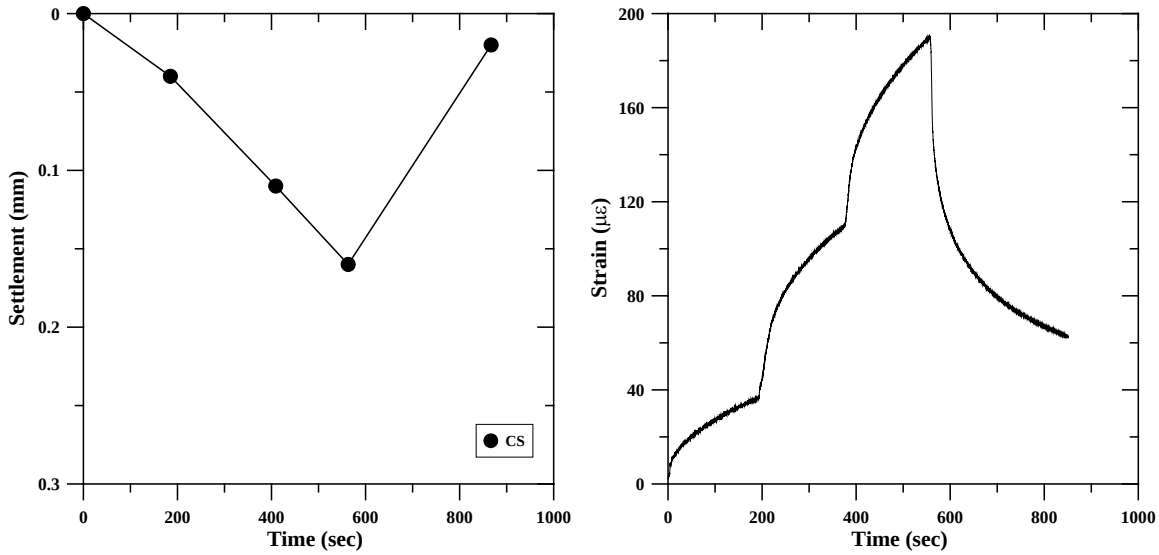

Figure 4. Settlement and strain response in control section.

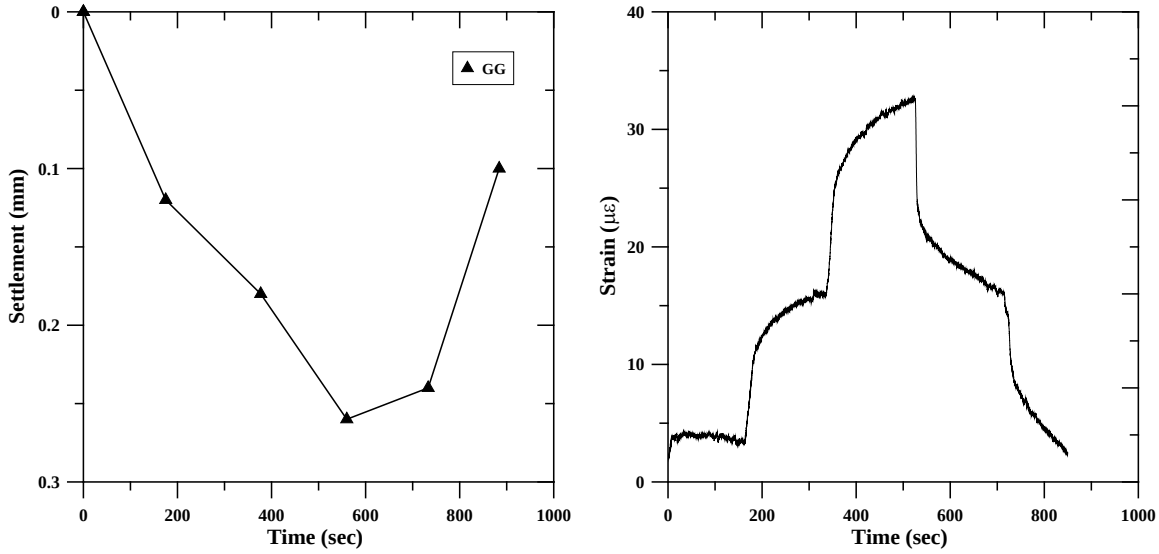

Figure 5. Settlement and strain response in geosynthetic-reinforced section.

Hence, to understand this condition, a typical load and unload stage was considered for the control and geosynthetic-reinforced sections, as shown in Fig. 6. It can be seen that the slope of the strain-time curve for both load and unload stages are steep indicating the settlement and strains recorded under an applied load after 120 seconds of wait period was not completely stabilized. The displacement transducers adopted with the PLT device to record the settlements were not able to record continuous displacements at micro-level and only the ultimate settlement at the end of each loading and unloading stage was recorded. On the other hand, the strain gauges adopted in the study were capable of recording the strain values on the order of micro-strains, suggesting to adopt waiting periods longer than that prescribed in DIN 18134:2012-04. It should also be noted

that the slope of ‘Time-strain’ curve for geosynthetic-reinforced section looks flat in comparison to the control section, due to the high strains recorded in the latter case.

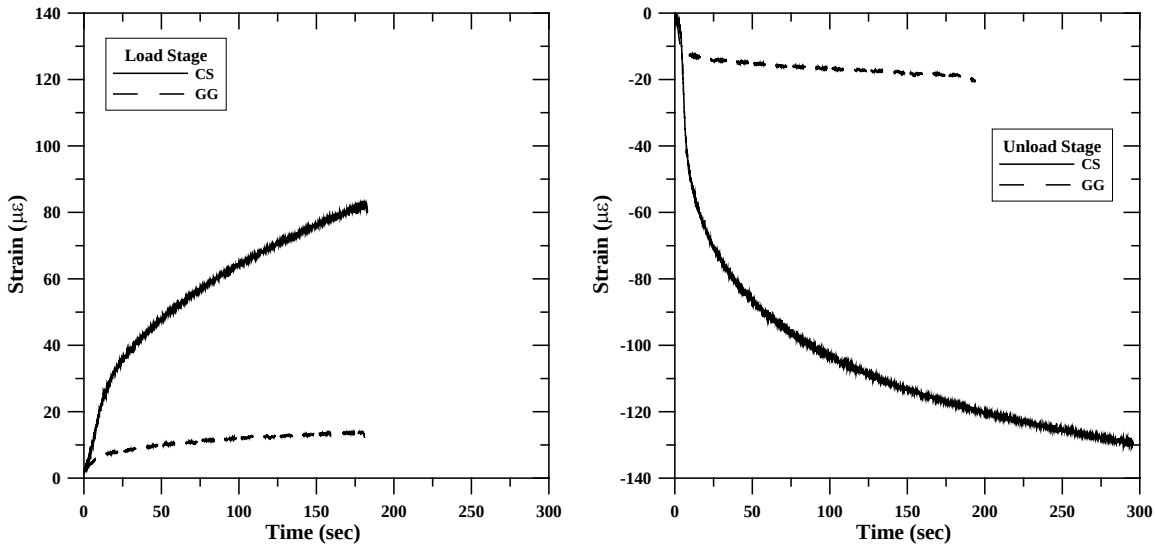

Figure 6. Typical loading and unloading stages of static PLT.

Figure 7 shows the settlement and strain responses for three loading stages adopted in the second phase (i.e., after overlay construction) of testing in this study and it can be observed that the settlement and strains increased with an increase in the applied load. The settlement in the control section is consistently lower than that of the geosynthetic-reinforced section, while the strains in the control section are consistently higher than that of the geosynthetic-reinforced section. As previously discussed, this may be due to the influence of asphalt surface temperature and the pre-existing pavement conditions. The influence of asphalt surface temperature and the pre-existing conditions on the surface settlement and asphalt strains are discussed in the sections below.

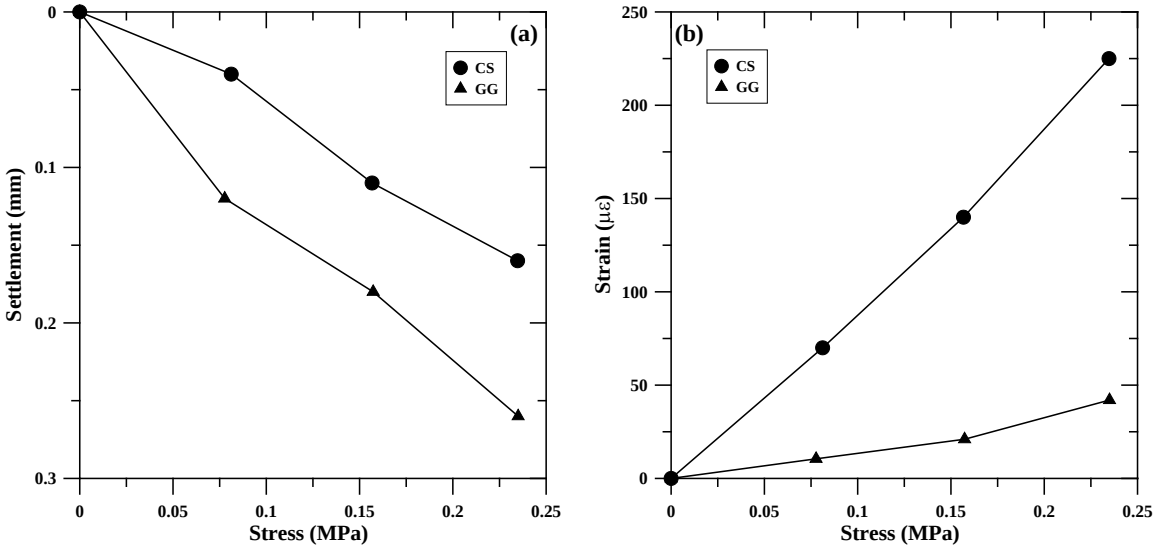

Figure 7. Settlement and strain responses under different loading stages (as recorded).

Influence of Temperature.

It is well known that the asphalt mixes are viscoelastic under small strain conditions, which is a function of time and temperature (Witczak and Solti 2004; Hu et al. 2019). The ambient and asphalt surface temperatures greatly influence the resilient modulus of asphalt layer and changes in the modulus influence the surface settlement and the tensile strains within the asphalt layer. Hence, to completely characterize the asphalt mixture adopted in the study, dynamic modulus tests were conducted at different temperatures of 14 °F, 40 °F, 70 °F, 100 °F, and 130 °F, and different frequencies of 0.1 Hz, 0.5 Hz, 1 Hz, 5 Hz, 10 Hz, and 25 Hz. Subsequently, a dynamic modulus master curve was developed, as shown in Fig. 8. The dynamic modulus master curve is often described by a sigmoidal function as follows (Witczak and Solti 2004; Hu et al. 2019):

$$log|E^*| = \delta + \frac{\alpha}{1+e^{\beta+\gamma log t_r}} \quad (1)$$

where, δ is the minimum value of $log|E^*|$ in the sigmoid function; α is the vertical span of the function; β and γ are shape parameters for the sigmoid curve; and t_r is the reduced loading time.

Based on the time-temperature superposition principle, $log\ t_r$ in Eq. 1 can be expressed as:

$$log t_r = log\ t - log a_T \quad (2)$$

where, t is the actual loading time at a given temperature (T); a_T is the temperature shift factor. The time-temperature shift factor can be fitted by a second order polynomial as shown in Fig. 8b.

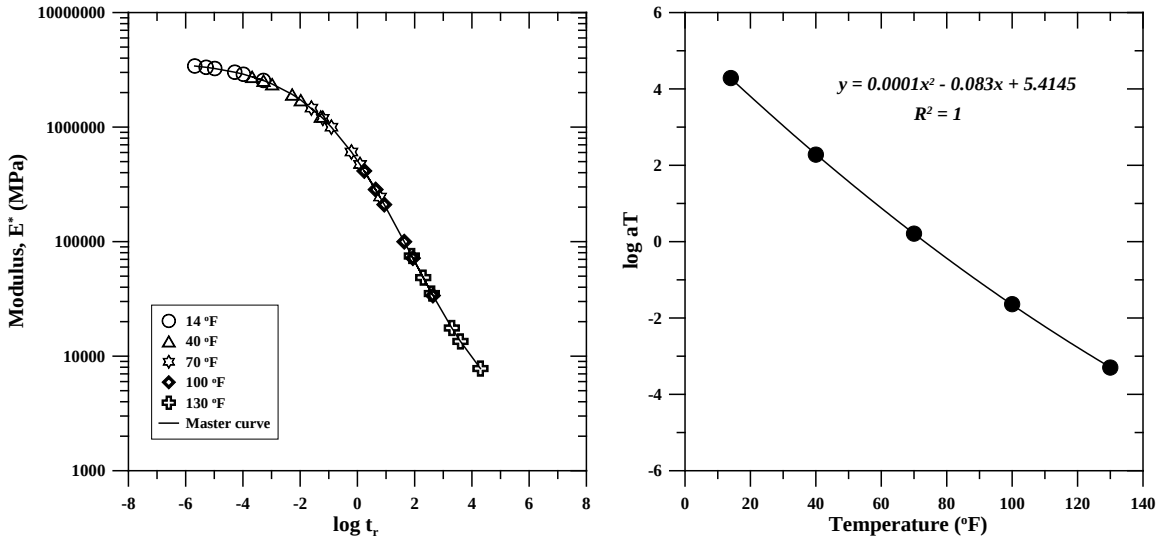

Figure 8. Dynamic Modulus Master Curve of the asphalt mixture used in the study.

From Fig. 8 and Eq. 1, the dynamic modulus of the asphalt mixture adopted in the study could be estimated for different temperatures between 14 °F and 130 °F and different frequencies (load time) between 0.01 Hz (10 secs) and 25 Hz (0.04 secs). However, to understand the influence of dynamic modulus of asphalt concrete on the surface settlement and asphalt strains at a depth of 6 inches, multi-layer linear elastic analysis (MLEA) was performed. The MLEA was performed

considering a pavement model with an overall asphalt layer of 8.5 inch thickness (3 inch overlay and 5.5 inch old asphalt), base and subbase layer of 16 inch thickness and infinite thickness for subgrade soil. The modulus input values for all the pavement layers was adopted based on the back-calculated modulus values predicted from the falling-weight deflectometer (FWD) test results. The MLEA was repeated for different modulus values of asphalt layer ranging from 70 MPa to 68,950 MPa and the corresponding surface settlements and tensile strains at a depth of 6 inch were estimated and plotted as shown in Fig. 9. A power function was separately fitted to 'Modulus-Settlement' (Fig. 9a) and 'Modulus-Tensile strain' (Fig. 9b) values, as shown in Equations 3 and 4. These equations can fairly estimate the surface settlement and tensile strain values for any asphalt modulus values ranging from 70 MPa to 68950 MPa.

$$\Delta = 3.9849(E')^{-0.349} \quad (3)$$

$$\varepsilon_{xx} = 0.0531(E')^{-0.924} \quad (4)$$

where, Δ is the surface settlement in mm; E' is the modulus of asphalt layer in MPa; and ε_{xx} is the tensile strain at a depth of 6 inch in the asphalt layer.

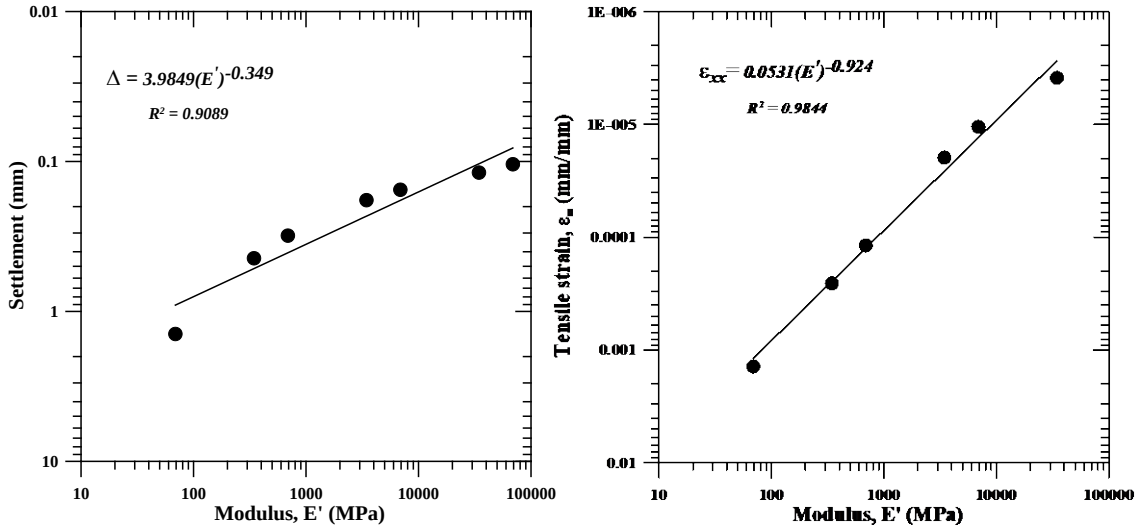

Figure 9. Multi-layer linear elastic analysis: (a) Variation of surface settlement with modulus of asphalt layer; (b) Variation of tensile strain (depth of 6 inch) with modulus of asphalt layer.

Since the asphalt surface temperature was different for the static PLT performed on the control and geosynthetic-reinforced pavement sections, a reference temperature of 77 °F was chosen. The modulus value corresponding to reference temperature of 77 °F was estimated to be 217,170 MPa, using Eq. 1 and Fig. 8. The estimated modulus value was then adopted in Equations 3 and 4 and the corresponding settlement and tensile strains were estimated to be 0.054 mm and 6.22×10^{-7} mm/mm, respectively. Similarly, the modulus values corresponding to test temperatures of 59 °F and 72 °F were estimated to be 575,610 MPa and 282,648 MPa, respectively. Subsequently, the settlement and strains corresponding to the modulus values at 59 °F and 72 °F were estimated to be 0.0389 mm and 2.53×10^{-7} mm/mm, and 0.0498 mm and 4.88×10^{-7} mm/mm, respectively, in the control and geosynthetic-reinforced sections. Eventually, temperature

correction factors for the surface settlements and tensile strains were determined separately for the control and geosynthetic-reinforced sections, based on the ratio of estimated settlement and tensile strain values at the reference temperature to that of the test temperature. The correction factors were then multiplied to the corresponding settlement and tensile strain values in the control and geosynthetic-reinforced sections. Fig. 10 presents the settlement and tensile strain response for different loading stages adopted in the study, normalized to a reference temperature of 77 °F. It can be observed that the tensile strains in both control and geosynthetic-reinforced sections are now increased to 560 με and 55 με from 225 με and 45 με, respectively. Similarly, an increase in the settlement of the control and geosynthetic-reinforced sections was observed from 0.16 mm and 0.26 mm to 0.24 mm and 0.29 mm, respectively. However, it should also be noted that the settlements in the control section are consistently lower than that of the geosynthetic-reinforced section, while the tensile strain trends suggest otherwise. This condition could be due to the pre-existing condition of the pavement sections, which is discussed below.

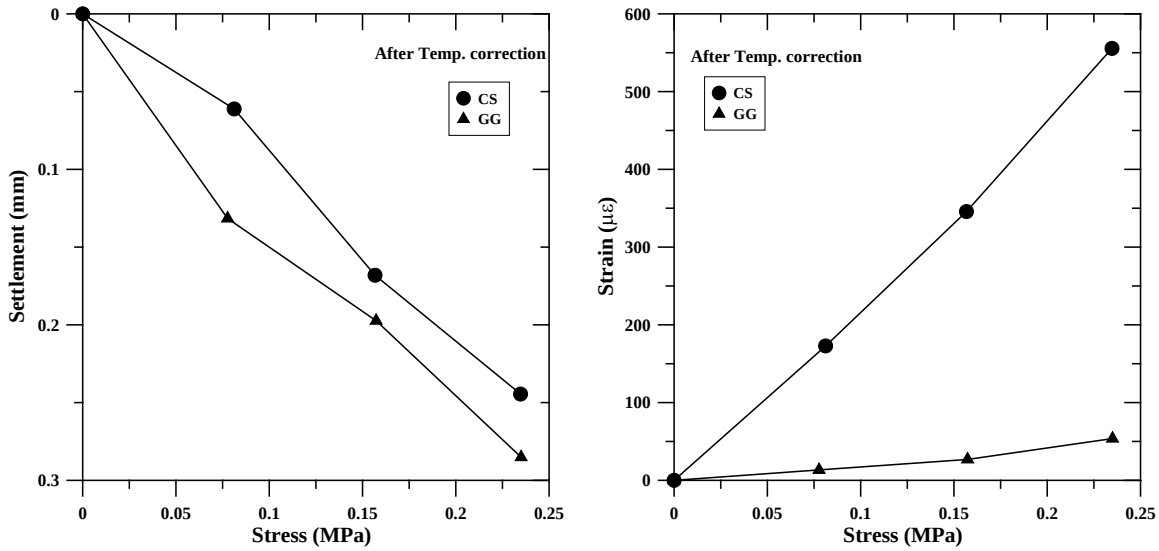

Figure 10. Settlement and strain response under different loading stages (after temperature correction).

Influence of pre-existing conditions.

The influence of pre-existing conditions of the pavement sections before the overlay construction is an important parameter to understand and fairly evaluate the performance of geosynthetic-reinforced section against the control section. Hence, to address the influence of pre-existing pavement conditions, static PLT performed on the old pavement prior to the installation of asphalt strain gauge and overlay construction, as discussed under 'Experimental Program,' has been considered. It should also be noted that only settlement response was recorded from the PLTs performed on the old pavement, but not strain response.

A maximum static plate load corresponding to a stress of 0.24 MPa was considered in the study, even though a maximum stress of 0.50 MPa was applied on the old pavement, to have a fair comparison between the PLTs performed on the old pavement and overlay. Fig. 11 presents the settlement response of the old pavement on which the control and geosynthetic-reinforced overlay sections were constructed. The PLTs were performed at different temperatures during this phase of testing as well, hence, a temperature correction corresponding to a reference temperature of 77

°F was applied to Fig. 11a and resulted in Fig. 11b. It can be observed that the settlements in old pavement below the control section are consistently lower than that of old pavement below the geosynthetic-reinforced section, suggesting a better settlement response in the control section.

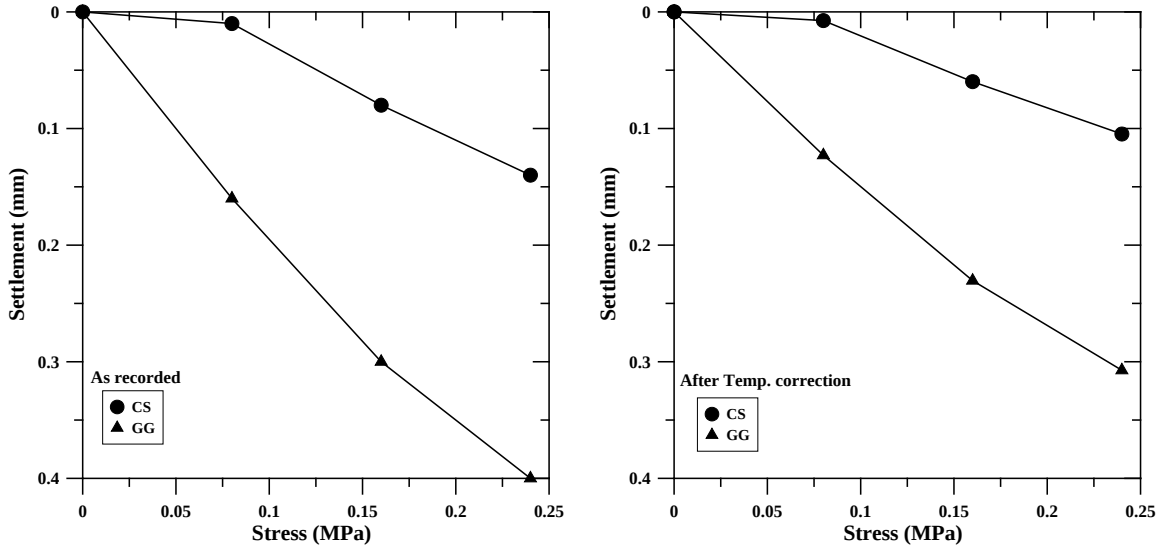

Figure 11. Settlement response of pavement section before overlay construction: (a) as recorded; (b) after temperature correction.

Besides, to understand the influence of pre-existing pavement conditions on the settlement response of the control and geosynthetic-reinforced sections, the settlements from Fig. 11b and Fig. 10a were compared and the percentage reduction were determined, as plotted in Fig. 12a. Similarly, from Fig. 10b, the reduction in tensile strains in the geosynthetic-reinforced section with respect to the control section was determined, irrespective of pre-existing pavement condition and plotted, as shown in Fig. 12b.

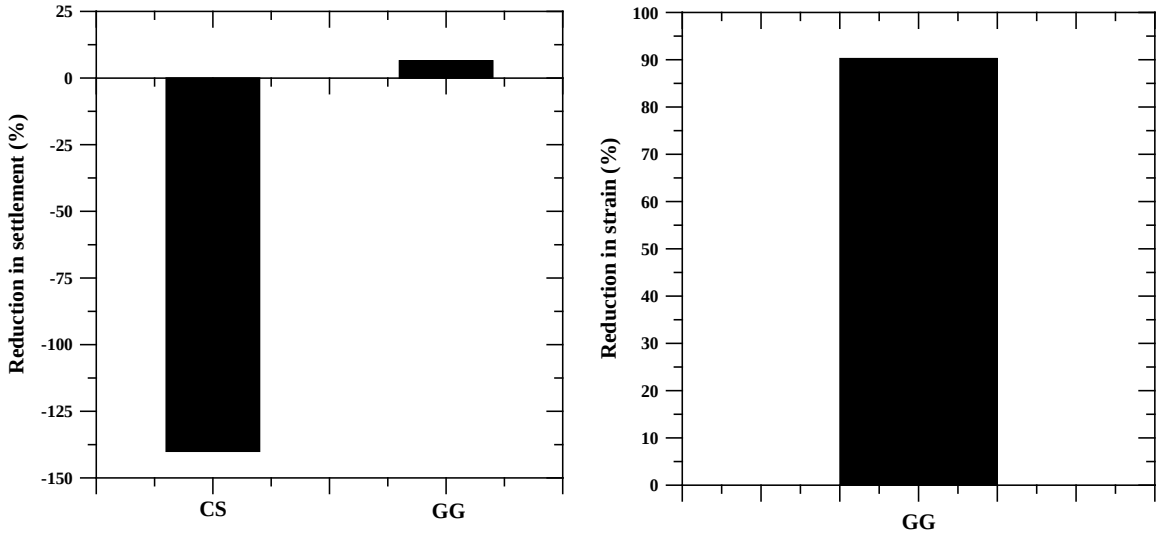

Figure 12. (a) Percentage reduction in settlement; (b) Percentage reduction in tensile strain.

It can be observed that the plate settlement on asphalt overlay increased by 140% compared to the plate settlement on the old pavement in the control section. While, the plate settlements on the asphalt overlay reduced by 6.5% compared to that on the old pavement in the geosynthetic-reinforced section. The important observation in the control section suggests that the oxidation of old pavement resulted in a stiffer and brittle asphalt layer compared to the fresh resilient asphalt overlay, hence higher settlements in the latter case. However, the geosynthetic reinforcement provides enough stiffness and resilience to the asphalt layers and effectively resist the settlements under the plate loads. In addition, a reduction in tensile strain by 90% was witnessed in the geosynthetic-reinforced section, irrespective of pre-existing pavement condition.

Overall, it can be summarized that the geosynthetic reinforcement adopted in the study was effective in resisting the plate settlements and minimizing the critical tensile strains responsible for asphalt cracking.

CONCLUSION

In this study, the plate settlement and asphalt strain responses in full-scale field test sections comprising both unreinforced (control) and geosynthetic-reinforced asphalt overlay test sections was evaluated using static plate load tests. The following conclusions can be drawn from the study:

The asphalt strain gauges adopted in the study were capable of measuring the influence of plate loads on the order of micro strains, suggesting a waiting period greater than 120 seconds between successive load/unload stages during a static plate load test.

The plate settlements and asphalt strains recorded under the static plate loads suggest a significant influence of the asphalt surface temperature and the pre-existing condition of the pavement sections on their responses.

The plate settlements on the overlay was found to be 140% higher than that on the old pavement in the control section, owing to the oxidation of the old asphalt resulting in a stiffer and brittle asphalt layer.

The geosynthetic reinforcement provided additional flexural stiffness and resilience to the asphalt layers and the geosynthetic-reinforced section effectively resisted the settlement under the plate loads.

A reduction of 90% in the tensile strain was quantified in the geosynthetic-reinforced section against the control section, irrespective of the pre-existing pavement conditions.

Overall, it can be summarized that the geosynthetic-reinforcement adopted in the study was effective in resisting the plate settlements and minimizing the critical tensile strains responsible for asphalt cracking.

ACKNOWLEDGEMENTS

The authors wish to thank the Texas Department of Transportation (TxDOT) for financial support of this study.

REFERENCES

Canestrari, F., Ferrotti, G., Partl, M.N. and Santagata, E. (2005). Advanced testing and characterization of interlayer shear resistance, *Transportation Research Record*, 1929:69-78.

Correia, N. S. and J. G. Zornberg (2016). Mechanical response of flexible pavements enhanced with geogrid-reinforced asphalt overlays. *Geosynthetics International,* 23 (3):183–193.

DIN 18134:2012-04 (2012). Soil Testing procedures and testing equipment- Plate load test. *Deutscnes Institut fur Norrnung e. V.*, Berlin, Beuth Verlag Gmbh, Berlin, Germany.

Hu, S., Rahman, A., Zhang, J., Zhou, F. and Scullion, T. (2019). *Implementation of Texas Mechanistic-Empirical Flexible Pavement Design System (TxME),* Project Report, FHWA Project TX-18/5-6622-01-R1: Texas A&M Transport Institute, College Station, Texas.

Khodaii, A., Fallah, S. and Nejad, F.M. (2009). Effects of geosynthetics on reduction of reflection cracking in asphalt overlays, *Geotextiles and Geomembranes*, Elsevier Science Publishers Ltd, England, 27(1):1-8.

Kumar, V.V. and Saride, S. (2017). Use of Digital Image Correlation for the Evaluation of Flexural Fatigue Behavior of Asphalt Beams with Geosynthetic Interlayers, *Transportation Research Record*, 2631:55-64.

Kumar, V.V., Saride, S. and Peddinti, P.R.T. (2017). Interfacial Shear Properties of Geosynthetic Interlayered Asphalt Overlays, *Geotechnical Frontiers-2017,* Orlando, Florida, ASCE, GSP-277, 442-451.

Leutner, R. (1979). Untersuchung des Schichtverbundes beim bituminösen Oberbau, (In German) *Bitumen,* Hamburg, Germany, 3.

Lytton, R.L. (1989). Use of Geotextiles for Reinforcement and Strain Relief in Asphalt Concrete, *Geotextiles and Geomembranes*, Elsevier Science Publishers Ltd, England, 8:217-237.

Montestruque, G., Rodrigues, R., Nods, M. and Elsing, A. (2004). Stop of reflective crack propagation with the use of PET geogrid as asphalt overlay reinforcement, *5th RILEM Conference on Cracking in Pavements*, Limoges, France, RILEM Publications S.A.R.L., 231-238

Roodi, G.H., Morsy, A.M. and Zornberg, J.G. (2017). Experimental Evaluation of the Interaction between Geosynthetic Reinforcements and Hot Mix Asphalt, *International Conference on Airfield and Highway Pavements,* ASCE, Philadelphia, Pennsylvania, USA, 428-439.

Saride, S. and Kumar, V.V. (2019). Estimation of Service life of Geosynthetic-Reinforced Asphalt Overlays from Beam and Large-Scale Fatigue Tests, *Journal of Testing and Evaluation*, 47(4): 2693-2716.

TxDOT. 2014. Standard Specifications for Construction and Maintenance of Highways, Streets, and Bridges. *Texas Department of Transportation,* Austin, Texas, USA.

West, R.C., Zhang, J. and Moore, J. (2005). Evaluation of bond strength between pavement layers, *NCAT Report 05-08, National Center for Asphalt Technology*, Auburn, AL.

Witczak, M.W. and A. Solti. (2004). *A Recommended Methodology for Developing Dynamic Modulus E* Master Curves from Non-Linear Optimization,* Project Report, NCHRP Project 9-19: Arizona State University, Tempe, Arizona.

Zou, W., Wang, Z. and Zhang, H. (2007). Field Trial for Asphalt Pavements Reinforced with Geosynthetics and Behavior of Glass-Fiber Grids, *Journal of Performance of Constructed Facilities*, ASCE, 21(5):361-367.